Numer. Math. Theor. Meth. Appl.
doi: 10.4208/nmtma.OA-2025-0019

Vol. **19**, No. 1, pp. 1-19
February 2026

A Highly Efficient USOR-Like Iterative Method for the Stationary Wigner Equation with Scattering

Yidan Wang[1], Haiyan Jiang[1,*], Tiao Lu[2,3] and Wenqi Yao[4]

[1] *School of Mathematics and Statistics, Beijing Institute of Technology, Beijing 100081, P.R. China*
[2] *CAPT, LMAM, School of Mathematical Sciences, Peking University, Beijing 100871, P.R. China*
[3] *Chongqing Research Institute of Big Data, Peking University, Chongqing 401121, P.R. China*
[4] *School of Mathematics, South China University of Technology, Guangzhou 510641, P.R. China*

Received 23 February 2025; Accepted (in revised version) 5 July 2025

Abstract. The stationary Wigner equation (SWE) is often used to model the quantum transport in semiconductor devices. The discrete stationary Wigner equation is derived using the first-order upwind scheme and the sinc-Galerkin method [H. Jiang, T. Lu, and W. Zhang, J. Comput. Appl. Math. 409 (2022), 114152]. Based on the successive over relaxation (SOR) iterative method, we develop the basic SOR-like (BSOR-like) and updated SOR-like (USOR-like) iterative methods for solving the discrete stationary Wigner equation efficiently. The main difference between these two iterative methods is that the USOR-like iterative method aims to make more use of the updated components of the Wigner function by splitting the pseudo-differential term. The convergence range of the relaxation parameter in the USOR-like iterative method is numerically investigated. Compared with that of the BSOR-like iterative method, this interval is significantly enlarged. Numerical results have also shown that the USOR-like iterative method is more computationally efficient than the BSOR-like iterative method. As an application, the resonant tunneling effect and the effects of scattering are investigated by simulating a resonant tunneling diode (RTD) using the USOR-like iterative method.

AMS subject classifications: 65F10, 81S30

Key words: Stationary Wigner equation, iterative method, resonant tunneling diode, SOR method, convergence condition.

*Corresponding author. *Email addresses:* yidanwang@bit.edu.cn (Y. Wang), hyjiang@bit.edu.cn (H. Jiang), tlu@pku.edu.cn (T. Lu), yaowq@scut.edu.cn (W. Yao)

1. Introduction

The Wigner equation was derived by Wigner [29] as a quantum correction of classical statistical mechanics for low temperatures. Given its similarity to the Boltzmann transport equation [13, 17], the Wigner equation can deal with the inflow boundary conditions [8] and the scattering mechanism well. The Wigner equation has been applied in many fields, such as quantum optics [11] and semiconductor devices [8]. In the steady-state simulation of a given quantum system, one needs to design schemes with good stability and high precision when utilizing the transient Wigner equation. By means of the stationary Wigner equation, one no longer pays attention to the transient state. Solving the SWE numerically is equivalent to solving a large system of equations. The computational complexity of direct solvers, such as the Gaussian elimination, could be significantly larger than that of excellent iterative methods. Therefore, constructing an efficient iterative method is crucial for numerically solving the SWE.

Numerical methods for solving the stationary Wigner inflow boundary value problem have been widely and deeply explored for decades. The finite difference methods [8,13] and a weighted essentially non-oscillatory (WENO)-solver [7] are proposed for the discretization of the advection term in the Wigner equation. Many methods with high accuracy, e.g., the spectral collocation method [24], the spectral element method [25], and the sinc-Galerkin method [15], are adopted to discretize the Wigner equation in k-space. By employing the Fourier pseudo-spectral method, the authors derive the stationary discrete velocity Wigner equation and prove its well-posedness in [1]. The parity decomposition is adopted in [2, 19] to reduce the SWE with the inflow boundary conditions to an initial problem, and the partial problem is proved to be well-posed. In [20], the moment system for the Wigner equation derived in [4] is numerically solved using the NRxx method and the finite volume method. Considering the singularity at zero velocity, a singularity-free numerical scheme based on an equivalent form of the SWE is proposed, and the numerical convergence with respect to the velocity mesh size is obtained [21]. The SWE can be solved together with a Poisson equation. Convergence may be achieved via the decoupled Gummel method [3, 10] or the fully coupled Newton iterative method [3, 14]. Because of the similarity to the Boltzmann equation, the Wigner equation can be solved with the Monte Carlo (MC) method [18,22,27]. In [26], the authors model the stationary Wigner inflow boundary value problem as an optimization problem, which is solved with the shooting algorithm. The imaginary time propagation method combined the finite element method is used to solve an eigenvalue problem for the stationary Wigner function [31].

Analogous to solving a system of linear equations using an iterative method, constructing an iterative method for solving the discrete SWE is an alternative way. For some problems, the successive over relaxation iterative method, which immediately replaces the old component with the newly calculated one, could converge with a few iterations. The choice of the relaxation parameter ω has a significant influence on the convergence of the SOR iterative method. For solving a system of non-smooth equations, the SOR-Newton method is proposed and the choice of the relaxation parameter

ω for convergence is analyzed in [6]. In [28], the modified method is further investigated. For 3D Navier-Stokes equations on graphics processing units, a GPU-based multi-color SOR method is proposed, noticing that each color only needs the information of known values from either the already updated color or the previous iteration [30]. In this paper, the first-order upwind scheme and the sinc-Galerkin method are applied to discretize the SWE as used in [15], subsequently resulting in the fully discretized system. Drawing inspiration from the core idea of the SOR iterative method, which involves updating the computed components in real-time during calculations, we design the updated SOR-like iterative method for the SWE. The proposed USOR-like iterative method updates only the pseudo-differential term in real-time, while an implicit method is still adopted to discretize the advection term. This maintains the iterative stability (with a large relaxation parameter) as much as possible while keeping the low computational cost like an explicit scheme (without solving a system of equations).

The resonant tunneling diode is studied by utilizing the new iterative method, and the main features of the RTD are explored successively. As one of the most important quantum devices, an RTD [5, 23] is usually simulated to explore some typical quantum phenomena, such as the negative differential region (NDR) of I-V curves, the resonant tunneling effect and the influence of scattering [3, 9, 12, 13]. In [9], the effects of scattering on I-V characteristics of the RTD are investigated using the Boltzmann collision operator, which include the peak-to-valley ratio, the profile of the conduction band edge, and the transient response [13]. In this paper, we compare the convergence range between the basic SOR-like and the USOR-like iterative methods. The numerical results show the USOR-like iterative method improves the convergence range and the computational efficiency. By using the USOR-like iterative method, the resonant tunneling effect is simulated successfully. Meanwhile, we investigate how the scattering affects I-V characteristics of the RTD. The effects of scattering are explained using the Wigner distribution function, where contour lines of the Wigner function provide visual assistance, as demonstrated in [12, 13].

The rest of this paper is organized as follows. We introduce the SWE briefly in Section 2. Section 3 presents the numerical methods to discretize the SWE and proposes the BSOR-like and USOR-like iterative methods. In Section 4, we compare the convergence of the two methods and simulate an RTD with the USOR-like method successfully, where some typical quantum phenomena and relevant discussions are given. The final conclusions are drawn in Section 5.

2. Mathematical model

The distribution of electrons in quantum devices can be described using the one-dimensional SWE with phonon scattering

$$\frac{k\hbar}{m^*}\frac{\partial f(x,k)}{\partial x} + \theta[f](x,k) = S[f](x,k), \quad (x,k) \in [0,L] \times (-\infty,\infty),$$

$$
\begin{aligned}
&\theta[f](x,k) = \int_{-\infty}^{+\infty} V_w(x,k-\eta) f(x,\eta) d\eta, \\
&V_w(x,k) = \frac{\mathrm{i}}{2\pi\hbar} \int_{-\infty}^{+\infty} V_{diff}(x,y) \exp(-\mathrm{i}ky) dy, \\
&V_{diff}(x,y) = V\left(x+\frac{y}{2}\right) - V\left(x-\frac{y}{2}\right), \\
&S[f](x,k) = \frac{1}{\tau}\left(\int_{-\infty}^{\infty} f(x,k')dk' f^{eq}(x,k) - f(x,k)\right),
\end{aligned}
\tag{2.1}
$$

where L denotes the total length of the device, $f(x,k)$ denotes the Wigner function, $\hbar$ represents the reduced Planck constant, and m^* denotes the effective mass of the electron. $\theta[f](x,k)$ represents the pseudo-differential term, which is related to the potential energy $V(x)$. $V(x)$ consists of the conduction band energy $V_c(x)$ and the static electric potential energy $V_s(x)$, i.e.,

$$
\begin{aligned}
V(x) &= V_c(x) + V_s(x), \\
V_s(x) &= -U(x)q,
\end{aligned}
$$

where q denotes the charge of the electron, and $U(x)$ denotes an external potential. $U(x)$ is usually set as constant at both ends of the device, which specifically reads $U(0) = 0$(V) and $U(L) = U_b$, where U_b denotes the applied bias. $S[f](x,k)$ models the effects of scattering, where τ represents the relaxation time and $f^{eq}(x,k)$ denotes the normalized equilibrium distribution under $U_b = 0$(V). We equip (2.1) with inflow boundary conditions proposed by Frensley in [8] at both ends, i.e.,

$$
\begin{cases}
f(0,k) = g_l(k), & k > 0, \\
f(L,k) = g_r(k), & k < 0
\end{cases}
$$

with

$$
\begin{aligned}
g_l(k) &= \frac{m^* k_B T_L}{\pi\hbar^2} \log\left(1 + \exp\left(\frac{\mu(0) - (\hbar^2 k^2)/(2m^*) - V(0)}{k_B T_L}\right)\right), \\
g_r(k) &= \frac{m^* k_B T_L}{\pi\hbar^2} \log\left(1 + \exp\left(\frac{\mu(L) - (\hbar^2 k^2)/(2m^*) - V(L)}{k_B T_L}\right)\right),
\end{aligned}
$$

where $\mu(x)$ denotes the Fermi energy, k_B represents the Boltzmann constant, and T_L denotes the temperature. The density functions of the electron and the current are derived by using the Wigner function $f(x,k)$ as

$$
\begin{aligned}
n(x) &= \frac{1}{2\pi} \int_{-\infty}^{\infty} f(x,k) dk, \\
J(x) &= \frac{q}{2\pi} \int_{-\infty}^{\infty} \frac{k\hbar}{m^*} f(x,k) dk,
\end{aligned}
$$

respectively.

3. Methodology

We adopt the sinc-Galerkin/finite-difference method [15] to discretize (2.1) in (x,k)-space, which leads to a large-scale sparse system of equations. A new iterative method is naturally proposed to solve this system of equations. The core idea of this method is to make greater use of the newly solved components during the process of solving the SWE according to a certain direction or sequence.

3.1. Discretizations of the SWE in (x,k)-space

We give a brief review of spatial discretization of (2.1), where a rigorous derivation could be found in [15]. Following [15], we use orthogonal basis $\{\phi_n(k)\}_{n=1,2,\ldots,N_k}$ to obtain the corresponding interpolation function $\tilde{f}(x,k)$ as the approximation of the Wigner function

$$f(x,k) \approx \tilde{f}(x,k) = \sum_{n=1}^{N_k} f(x,k_n)\phi_n(k), \tag{3.1}$$

where

$$\phi_n(k) = \frac{1}{\sqrt{\Delta k}}\mathrm{sinc}\left(\frac{k-k_n}{\Delta k}\right)$$

with

$$\mathrm{sinc}(x) = \frac{\sin(\pi x)}{\pi x}, \quad k_n = \frac{L_k}{2} + \left(\frac{1}{2} - n\right)\Delta k, \quad n = 1,\ldots,N_k, \quad \Delta k = \frac{L_k}{N_k}.$$

Substituting (3.1) in (2.1) and applying the Galerkin method to project the equation in $\mathrm{span}\{\phi_1,\phi_2,\cdots,\phi_{N_k}\}$, the following system is derived:

$$\begin{aligned}&\frac{k_j\hbar}{m^*}\frac{\partial f(x,k_j)}{\partial x} + \sum_{j'=1}^{N_k}\xi_{j-j'}(x)f(x,k_{j'})\\ &= \frac{1}{\tau}\left(\Delta k\sum_{j'=1}^{N_k} f(x,k_{j'})f^{eq}(x,k_j) - f(x,k_j)\right), \quad j = 1,\ldots,N_k,\end{aligned}$$

where

$$\xi_n(x) = \frac{\mathrm{i}\Delta k}{2\pi\hbar}\int_{-\pi/(\Delta k)}^{\pi/(\Delta k)} V_{diff}(x,y)\exp(\mathrm{i}n\Delta k y)dy. \tag{3.2}$$

Using the trapezoid rule, the discretized form of (3.2) is

$$\xi_n(x) \approx \xi_n^d(x) \triangleq -\frac{\Delta k\Delta y}{2\pi\hbar}\sum_{m=1}^{N_y} V_{diff}(x,y_m)\sin(n\Delta k y_m),$$

where

$$y_m = -\frac{\pi}{\Delta k} + m\Delta y, \quad m = 1,\ldots,N_y, \quad N_y\Delta y = \frac{2\pi}{\Delta k}.$$

Additionally, $N_k\Delta y = (2\pi)/(\Delta k)$ must be satisfied in order to preserve the mass conservation. We denote by f_{ij} the approximation of $f(x,k_j)$ at $x = x_i$, where $x_i = i\Delta x$, $i = 0,\ldots,N_x$, $\Delta x = L/N_x$. The first-order upwind scheme is applied to discretize the advection term, and the fully-discretized Wigner system (DWS) reads

$$\frac{k_j\hbar}{m^*}[Df]_{ij} + [\Theta f]_{ij} = [Sf]_{ij}, \quad i = 1,\ldots,N_x-1, \quad j = 1,\ldots,N_k, \tag{3.3}$$

where

$$[Df]_{ij} = \begin{cases} \dfrac{f_{ij} - f_{i-1,j}}{\Delta x}, & k_j > 0, \\ \dfrac{f_{i+1,j} - f_{ij}}{\Delta x}, & k_j < 0, \end{cases}$$

$$[\Theta f]_{ij} = \sum_{j'=1}^{N_k} \xi^d_{j-j'}(x_i) f_{ij'},$$

$$[Sf]_{ij} = \frac{1}{\tau}\left(\Delta k f^{eq}_{ij} \sum_{j'=1}^{N_k} f_{ij'} - f_{ij}\right).$$

At last, the discretized inflow boundary conditions are set as

$$\begin{cases} f_{0j} = g_l(k_j), & j = 1,\ldots,\dfrac{N_k}{2}, \\ f_{N_x j} = g_r(k_j), & j = \dfrac{N_k}{2}+1,\ldots,N_k. \end{cases}$$

3.2. The USOR-like iterative method

The discrete Wigner function is denoted by

$$F = (F_1, \cdots, F_{N_x-1})^\top,$$

where $F_i = (f_{i,1}, \cdots, f_{i,N_k}),\ i = 1,\ldots,N_x-1$. Denote by M_a, M_P and $M_S \in \mathbb{R}^{N\times N}$, where $N = (N_x-1)N_k$, the coefficient matrices in front of F, corresponding to the spatial discretization of $((k\hbar)/(m^*))((\partial f)/(\partial x))$, $\theta[f]$ and $S[f]$, respectively. In order to discuss iterative methods in a general way, (3.3) is rewritten in a matrix-vector form as follows:

$$(M_a + M_P + M_S)F = \boldsymbol{b},$$

where

$$M_a = \begin{pmatrix} K & -K_2 & & & & \\ -K_1 & K & -K_2 & & & \\ & -K_1 & K & -K_2 & & \\ & & \ddots & \ddots & \ddots & \\ & & & -K_1 & K & -K_2 \\ & & & & -K_1 & K \end{pmatrix},$$

$$
\begin{aligned}
M_P &= \mathrm{diag}(\Sigma_1, \Sigma_2, \cdots, \Sigma_{N_x-1}),\\
M_S &= \frac{1}{\tau}E_N + \tilde{M}_S,\\
\tilde{M}_S &= \mathrm{diag}(S_1, S_2, \cdots, S_{N_x-1}),
\end{aligned}
$$

and

$$
\boldsymbol{b} = \left(\boldsymbol{b}_1, \mathbf{0}, \cdots, \mathbf{0}, \boldsymbol{b}_{N_x-1}\right)^\top,
$$

where E_N is the N-th order identity matrix. Elements of M_a, M_P and $\tilde{M}_S$ are N_k-th order matrices, where

$$
\begin{aligned}
K &= K_1 + K_2,\\
K_1 &= \frac{\hbar}{m^*\Delta x}\mathrm{diag}\left(k_1, \cdots, k_{N_k/2}, 0, \cdots, 0\right),\\
K_2 &= -\frac{\hbar}{m^*\Delta x}\mathrm{diag}\left(0, \cdots, 0, k_{N_k/2+1}, \cdots, k_{N_k}\right),
\end{aligned}
$$

$$
\Sigma_i = \begin{pmatrix}
\xi^d_{i,0} & \xi^d_{i,-1} & \xi^d_{i,-2} & \cdots & \xi^d_{i,1-N_k}\\
\xi^d_{i,1} & \xi^d_{i,0} & \xi^d_{i,-1} & \cdots & \xi^d_{i,2-N_k}\\
\vdots & \vdots & \vdots & \ddots & \vdots\\
\xi^d_{i,N_k-1} & \xi^d_{i,N_k-2} & \xi^d_{i,N_k-3} & \cdots & \xi^d_{i,0}
\end{pmatrix}_{N_k\times N_k},
$$

$$
S_i = -\frac{\Delta k}{\tau}\begin{pmatrix}
f^{eq}_{i,1} & f^{eq}_{i,1} & \cdots & f^{eq}_{i,1}\\
f^{eq}_{i,2} & f^{eq}_{i,2} & \cdots & f^{eq}_{i,2}\\
\vdots & \vdots & \ddots & \vdots\\
f^{eq}_{i,N_k} & f^{eq}_{i,N_k} & \cdots & f^{eq}_{i,N_k}
\end{pmatrix}_{N_k\times N_k},
$$

and $\xi^d_{i,j-j'} = \xi^d_{j-j'}(x_i)$. Elements of $\boldsymbol{b}$ are N_k-th order vectors, viz.

$$
\begin{aligned}
\boldsymbol{b}_1 &= \frac{\hbar}{m^*\Delta x}\left(k_1 f_{0,1}, \cdots, k_{N_k/2} f_{0,N_k/2}, 0, \cdots, 0\right),\\
\boldsymbol{b}_{N_x-1} &= -\frac{\hbar}{m^*\Delta x}\left(0, \cdots, 0, k_{N_k/2+1} f_{N_x,N_k/2+1}, \cdots, k_{N_k} f_{N_x,N_k}\right).
\end{aligned}
$$

Constructing a system of equations with the same solution and determining the iteration matrix is a key to the development of iterative methods for the system of linear equations. We denote by

$$
F^{(n)} = \left(F^{(n)}_1, \cdots, F^{(n)}_{N_x-1}\right)^\top,
$$

the discrete Wigner function for the DWS (3.3) at the n-th iteration, where

$$
F^{(n)}_i = \left(f^{(n)}_{i,1}, \cdots, f^{(n)}_{i,N_k}\right), \quad i = 1, \ldots, N_x - 1.
$$

The BSOR-like iterative method for the DWS (3.3) is designed as

$$F^{(n+1)} = F^{(n)} + \omega \left[-M_a F^{(n+1)} - M_P F^{(n)} - M_S F^{(n)} + \boldsymbol{b} \right], \tag{3.4}$$

where ω denotes the relaxation parameter, superscripts $(n+1)$ and (n) denote the current and previous iteration, respectively. If the effects of scattering are not included, the corresponding iterative method is

$$F^{(n+1)} = F^{(n)} + \omega \left[-M_a F^{(n+1)} - M_P F^{(n)} + \boldsymbol{b} \right]. \tag{3.5}$$

At each iteration, the sequence of solving is as illustrated in Fig. 1. For $k > 0$, we solve f_{ij} in sequence from $i = 1$ to $i = N_x - 1$ for each k_j from $j = 1$ to $j = N_k/2$; for $k < 0$, we solve f_{ij} in sequence from $i = N_x - 1$ to $i = 1$ for each k_j from $j = N_k$ to $j = N_k/2 + 1$. In Fig. 1, black points represent values of the Wigner function at the boundaries, corresponding to the inflow boundary conditions. Red and brown points are components that need to be solved at the current iteration. Green points are already updated elements at the same iteration, while blue points represent the elements that have not yet been solved at the current iteration. To improve the convergence, we make greater use of the already solved components from the same iteration when computing each component at the new iteration. These changes are reflected in the term $M_P F^{(n)}$. When solving $f_{ij}^{(n+1)}$ corresponding to red and brown points, values of already updated components at the current iteration corresponding to green points replace values of these components at the previous iteration in $M_P F^{(n)}$. Therefore, M_P splits into two separate matrices, i.e., $\tilde{M}_P$ and $M_P - \tilde{M}_P$. As a result, the USOR-like iterative method for the DWS (3.3) is obtained as follows:

$$F^{(n+1)} = F^{(n)} + \omega \left[\big(-M_a - \tilde{M}_P \big) F^{(n+1)} - \big(M_P - \tilde{M}_P + M_S \big) F^{(n)} + \boldsymbol{b} \right], \tag{3.6}$$

where

$$\tilde{M}_P = \operatorname{diag}\big(\tilde{\Sigma}_1, \cdots, \tilde{\Sigma}_{N_x-1}\big), \quad \tilde{\Sigma}_i = \big(\tilde{\Sigma}_{i,1}, \tilde{\Sigma}_{i,2}, \cdots, \tilde{\Sigma}_{i,N_k}\big)^\top,$$

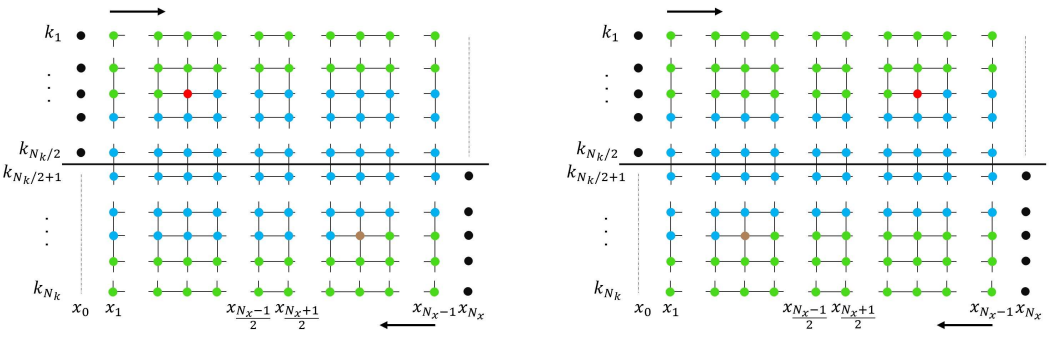

Figure 1: The order of solving the DWS at each iteration.

and

$$\tilde{\Sigma}_{i,j}=\begin{cases}\left(\xi^d_{i,j-1},\cdots,\xi^d_{i,1},0,\cdots,0,\xi^d_{i,2j-N_k-2},\cdots,\xi^d_{i,j-N_k}\right)^\top,\\ \qquad\qquad 1\le i\le\dfrac{N_x}{2},\quad 1\le j\le\dfrac{N_k}{2},\\ \left(\xi^d_{i,j-1},\cdots,\xi^d_{i,2j-N_k-1},0,\cdots,0,\xi^d_{i,-1},\cdots,\xi^d_{i,j-N_k}\right)^\top,\\ \qquad\qquad 1\le i\le\dfrac{N_x}{2},\quad \dfrac{N_k}{2}<j\le N_k,\\ \left(\xi^d_{i,j-1},\cdots,\xi^d_{i,1},0,\cdots,0,\xi^d_{i,2j-N_k-1},\cdots,\xi^d_{i,j-N_k}\right)^\top,\\ \qquad\qquad \dfrac{N_x}{2}<i\le N_x,\quad 1\le j\le\dfrac{N_k}{2},\\ \left(\xi^d_{i,j-1},\cdots,\xi^d_{i,2j-N_k},0,\cdots,0,\xi^d_{i,-1},\cdots,\xi^d_{i,j-N_k}\right)^\top,\\ \qquad\qquad \dfrac{N_x}{2}<i\le N_x,\quad \dfrac{N_k}{2}<j\le N_k.\end{cases}$$

And the USOR-like iterative method in the absence of scattering is obtained as follows:

$$F^{(n+1)}=F^{(n)}+\omega\left[\big(-M_a-\tilde{M}_P\big)F^{(n+1)}-\big(M_P-\tilde{M}_P\big)F^{(n)}+\boldsymbol{b}\right]. \tag{3.7}$$

Remark 3.1. The design of the USOR-like iterative method, including (3.6) and (3.7), is reasonable. Firstly, if the operators M_P and M_S act on $F^{(n+1)}$ entirely and directly, solving a system of equations will be unavoidable and time-consuming, which is caused by the existence of the integral terms in $\theta[f]$ and $S[f]$. Secondly, we do not split the operator M_S to make more use of the newly solved components as that done on M_P, as seen in (3.6). Considering the integral in $S[f]$, if we continue to split the operator $\tilde{M}_S$ to maximize the use of the newly solved components, we must recalculate the integral value after solving each component, which obviously increases the computational cost. Additionally, the second version of the USOR-like (USOR-like2) iterative method is proposed for comparison

$$\begin{aligned}F^{(n+1)}=&F^{(n)}\\&+\omega\left[\left(-M_a-\tilde{M}_P-\frac{1}{\tau}E_N\right)F^{(n+1)}-(M_P-\tilde{M}_P+\tilde{M}_S)F^{(n)}+\boldsymbol{b}\right].\end{aligned} \tag{3.8}$$

Though (3.8) does not increase the computational cost, such operations do not relax the convergence condition significantly compared with (3.6), which is verified by numerical simulations in Section 4.1.

4. Numerical results

In this section, we verify the good convergence of the USOR-like iterative method for the DWS and investigate the effects of scattering by simulating an RTD with the USOR-like iterative method. An RTD with parameters chosen by Jensen and Buot in

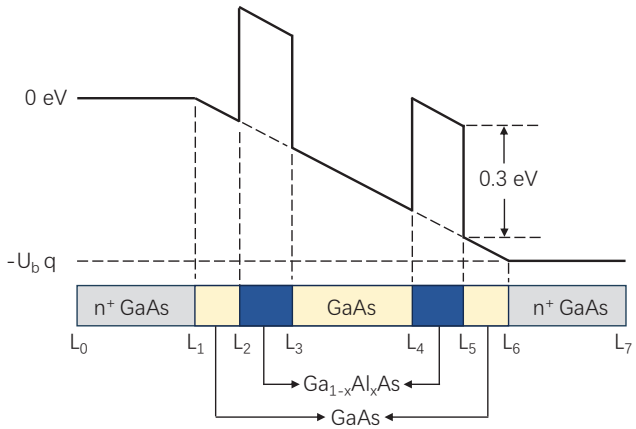

Figure 2: An RTD structure.

[13] is simulated, which has a heterostructure as shown in Fig. 2. We denote by L_{mn} the distance between L_m and L_n. As depicted in [13], the total length of the device is $L = L_{07} = 55$(nm), the length of two n^+GaAs regions (heavily doped) is $L_d = L_{01} = L_{67} = 19$(nm). The length of the two spacer regions is $L_{12} = L_{56} = 3$(nm), the length of the two potential barriers is $L_{23} = L_{45} = 3$(nm), and the length of the quantum well region is $L_{34} = 5$(nm). The doping concentration takes the value of 2×10^{-3} (nm^{-3}) inside two heavily doped regions while vanishes inside other regions (undoped). The conduction band energy is 0.3(eV) in $\mathrm{Ga}_{1-x}\mathrm{Al}_x\mathrm{As}$ and 0(eV) in GaAs. The temperature of the lattice T_L is set as 77(K), the relaxation time τ is 525.2(fs), the effective mass m^* is $0.0667m_0$ with m_0 the free electron mass and the permittivity ϵ is $12.9\epsilon_0$ with ϵ_0 the vacuum permittivity.

A linear constant external potential is equipped to the device, which reads

$$U(x) = \begin{cases} 0, & 0 \le x \le L_d, \\ \dfrac{x - L_d}{L - 2L_d} \times U_b, & L_d < x \le L - L_d, \\ U_b, & L - L_d < x \le L, \end{cases}$$

and we solve the DWS (3.3) iteratively for each applied bias till the steady-state solution is obtained. Specifically, the simulation proceeds for increasing U_b, from 0(V) to 0.4(V), with $\Delta U_b = 0.01$(V). When $U_b = 0$(V), iterations start from the equilibrium distribution

$$f^{(0)}(x,k) = \frac{m^* k_B T_L}{\pi\hbar^2} \log\left(1 + \exp\left(\frac{\mu(x) - (\hbar^2 k^2)/(2m^*) - V(x)}{k_B T_L}\right)\right),$$

and when $U_b > 0$(V), iterations start from the steady-state solution which corresponds to the last bias voltage $U_b - \Delta U_b$.

For arbitrary grid function $\boldsymbol{\nu} = (\nu_1, \cdots, \nu_m) \in \mathbb{R}^{1\times m}$, we define the L^2-norm of $\boldsymbol{\nu}$ as

$$\|\boldsymbol{\nu}\|_2 = \sqrt{\Delta x \sum_{i=1}^{m} \nu_i^2}.$$

The steady-state solution for each U_b is obtained when the following conditions:

$$\|\boldsymbol{J}^{(n+1)} - \boldsymbol{J}^{(n)}\|_2 \leq 10^{-9}, \quad \|\boldsymbol{n}^{(n+1)} - \boldsymbol{n}^{(n)}\|_2 \leq 10^{-9} \tag{4.1}$$

are satisfied, where

$$\boldsymbol{J}^{(n+1)} = \left(J_{1/2}^{(n+1)}, \cdots, J_{N_x-1/2}^{(n+1)}\right)$$

with

$$J_{i+1/2}^{(n+1)} = \frac{q\hbar\Delta k}{2\pi m^*}\left(\sum_{j=1}^{N_k/2} k_j f_{ij}^{(n+1)} + \sum_{j=N_k/2+1}^{N_k} k_j f_{i+1,j}^{(n+1)}\right),$$

and

$$\boldsymbol{n}^{(n+1)} = \left(n_0^{(n+1)}, \cdots, n_{N_x}^{(n+1)}\right)$$

with

$$n_i^{(n+1)} = \frac{\Delta k}{2\pi}\sum_{j=1}^{N_k} f_{ij}^{(n+1)}.$$

Once (4.1) is satisfied, we may regard the steady-state solution is obtained, and denote the corresponding current density by $\boldsymbol{J} = (J_{1/2}, \cdots, J_{N_x-1/2})$. Parameters associated with mesh grids are set as $N_k = 72$, $N_x = 110$ and $\Delta y = 2\Delta x$. To show electrical properties of the RTD, we study varying of the stable average current density versus increasing bias voltage, i.e., the I-V characteristic curve. Specifically, the stable average current density is defined according to

$$\bar{J} = \frac{1}{N_x}\sum_{i=0}^{N_x-1} J_{i+1/2}.$$

4.1. Convergence of the USOR-like iterative method

We compare the convergence of the USOR-like iterative method and two other methods proposed in Section 3. In the experiments, the stable average current densities $\bar{J}$ for $U_b \in [0, 0.4]$(V) with $\Delta U_b = 0.01$(V) are simulated with different ω. The interval of the relaxation parameter ω reflects the convergence condition. The required CPU times are collected in Tables 1 and 2.

For the case of no scattering, the results are shown in Table 1. The maximum of the allowed ω with the BSOR-like iterative method (3.5) is smaller than that with the USOR-like iterative method (3.7), which indicates that the latter relaxes the convergence condition compared with the former. When scattering is included, CPU times

Table 1: Comparison of the CPU times between the BSOR-like and USOR-like iterative methods when scattering is not included.

ω	2	1	0.5	0.2	0.1	0.05	0.02	0.01
BSOR-like	-	-	-	-	484.914s	550.645s	1034.3s	1491.94s
USOR-like	51.2893s	68.2471s	113.626s	163.549s	383.056s	425.238s	1150.43s	1582.48s

Table 2: Comparison of the CPU times among the BSOR-like, USOR-like and USOR-like2 iterative methods when scattering is included.

ω	2.5	2	1	0.5	0.2	0.1	0.05	0.02	0.01
BSOR-like	-	-	-	-	-	331.084s	513.566s	972.891s	1510.11s
USOR-like	-	31.7742s	44.0618s	94.4738s	219.119s	344.588s	454.459s	993.149s	1479.38s
USOR-like2	-	32.7836s	48.1941s	93.4895s	196.203s	336.257s	535.282s	981.457s	1514.34s

are listed in Table 2. From the results in Table 2, the USOR-like (3.6) and USOR-like2 (3.8) iterative methods relax the convergence condition compared with the BSOR-like iterative method (3.4), while there is no significant difference between the intervals of ω allowed by the USOR-like and USOR-like2 iterative methods. Actually, it verifies that splitting M_P into $M_P - \tilde{M}_P$ and $\tilde{M}_P$ significantly enhances its convergence. In contrast, splitting M_S into $\tilde{M}_S$ and $(1/\tau)E_N$ according to (3.8) does not notably improve the convergence, which highlights the effectiveness of operations on M_P. From the CPU times displayed in Tables 1 and 2, the USOR-like iterative method shows higher computational efficiency than the BSOR-like iterative method.

To provide more details on the convergence, we present the number of iterations required by the USOR-like and BSOR-like iterative methods to attain the same accuracy for different values of ω in Tables 3 and 4. These tables consider four distinct U_b values, namely 0.1(V), 0.3(V), 0.35(V) and 0.4(V). Specifically, Table 3 displays the results for the scattering-free case, while Table 4 outlines the results for the scattering-included

Table 3: Comparison of the iteration steps required by the BSOR-like and USOR-like iterative methods to attain the same accuracy when scattering is not included.

$\mathbf{U_b = 0.1(V)}$	Iterations		$\mathbf{U_b = 0.3(V)}$	Iterations	
ω	BSOR-like	USOR-like	ω	BSOR-like	USOR-like
0.05	8160	8162	0.05	3541	3097
0.1	4923	4927	0.1	2264	2102
0.5	-	1286	0.5	-	670
2	-	384	2	-	314
$\mathbf{U_b = 0.35(V)}$	Iterations		$\mathbf{U_b = 0.4(V)}$	Iterations	
ω	BSOR-like	USOR-like	ω	BSOR-like	USOR-like
0.05	3503	3179	0.05	3485	3020
0.1	2281	1939	0.1	2329	2050
0.5	-	660	0.5	-	649
2	-	463	2	-	629

Table 4: Comparison of the iteration steps required by the BSOR-like and USOR-like iterative methods to attain the same accuracy when scattering is included.

$\mathbf{U_b = 0.1(V)}$	Iterations		$\mathbf{U_b = 0.3(V)}$	Iterations	
ω	BSOR-like	USOR-like	ω	BSOR-like	USOR-like
0.05	7104	7105	0.05	3094	2746
0.1	4021	4018	0.1	2086	1885
0.5	-	1032	0.5	-	626
2	-	324	2	-	293
$\mathbf{U_b = 0.35(V)}$	Iterations		$\mathbf{U_b = 0.4(V)}$	Iterations	
ω	BSOR-like	USOR-like	ω	BSOR-like	USOR-like
0.05	3180	2286	0.05	4017	3974
0.1	2126	1939	0.1	2544	2517
0.5	-	631	0.5	-	778
2	-	332	2	-	434

case. For any of the methods mentioned here, the number of iterations required under a fixed applied bias voltage decreases with increasing ω. Whether or not scattering is included, the USOR-like iterative method takes fewer iterations than the BSOR-like iterative method with the same ω under large U_b, i.e., $U_b \geq$0.3(V). In addition, under the same applied bias voltage U_b, the iteration steps required by the USOR-like iterative method for large $\omega > 0.1$ are fewer than those required by the BSOR-like iterative method for small $\omega \leq 0.1$. The results in Tables 3 and 4 demonstrate the superior convergence rate of the USOR-like iterative method.

Figs. 3 and 4 show I-V curves simulated by the USOR-like and BSOR-like iterative methods with different ω. In Fig. 3(a), I-V curves under different ω using the BSOR-like

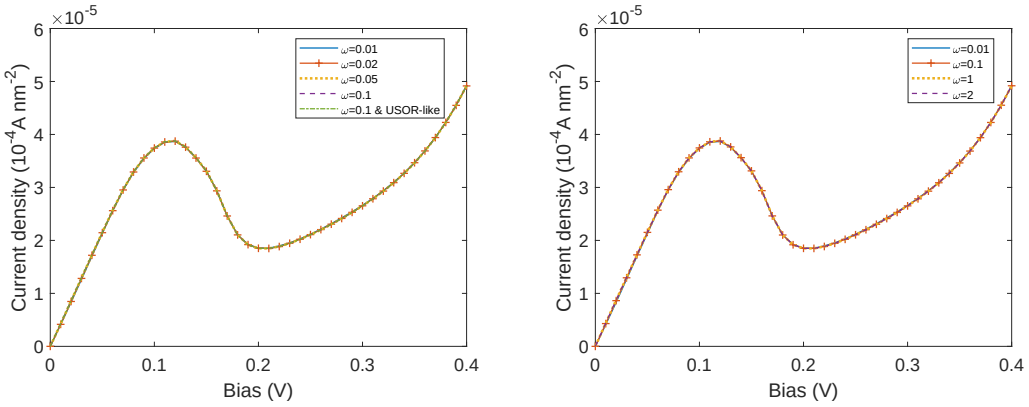

(a) BSOR-like iterative method (b) USOR-like iterative method

Figure 3: I-V curves with different ω in the absence of scattering. (a) The green line represents the I-V curve simulated using the USOR-like iterative method when $\omega = 0.1$, while the other curves are simulated using the BSOR-like iterative method with different ω. (b) I-V curves simulated using the USOR-like iterative method.

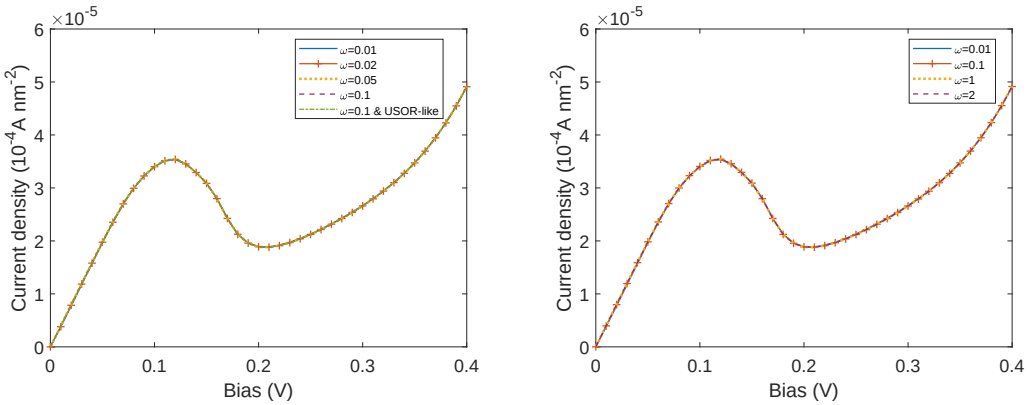

(a) BSOR-like iterative method (b) USOR-like iterative method

Figure 4: I-V curves with different ω in the presence of scattering. (a) The green line represents the I-V curve simulated using the USOR-like iterative method when $\omega = 0.1$, while the other curves are simulated using the BSOR-like iterative method with different ω. (b) I-V curves simulated using the USOR-like iterative method.

method almost coincide. Moreover, I-V curves obtained by the USOR-like and BSOR-like iterative methods are almost identical when $\omega = 0.1$. These observations can also be noticed in Fig. 4(a). The I-V curves simulated by the USOR-like iterative method, as presented in Figs. 3(b) and 4(b), are consistent for different values of ω. Considering the convergence rate, the USOR-like iterative method is employed, and the relaxation parameter ω is fixed to be 2 in the following numerical experiments. Additionally, the negative differential region is observed in each I-V curve.

4.2. The resonant tunneling effect of the RTD

In this section, we study the resonant tunneling effect of the RTD with and without scattering. We simulate I-V curves with (3.6) and (3.7) for $U_b \in [0, 0.4]$(V) in Fig. 5. $U_b = 0.12$(V) and $U_b = 0.21$(V) are bias voltages corresponding to the peak and the valley of the I-V curves, respectively. The other two bias voltages, i.e., $U_b = 0.05$(V) and $U_b = 0.16$(V), correspond to reaching half the height needed to climb to the peak from $U_b = 0$(V) and $U_b = 0.21$(V), respectively. In Fig. 5, compared to the case of no scattering, the peak current density decreases when scattering is included. In the higher bias region, where $U_b \geq 0.21$(V), scattering has no significant impact on the current density. This can be attributed to the fact that the distribution of electrons deviates greatly from the equilibrium distribution in high electric fields, making the relaxation time of electrons less well-defined [16].

Fig. 6 depicts the potential energy and the electron density under four bias values, i.e., 0.05(V), 0.12(V), 0.16(V) and 0.21(V), in both the presence and absence of scattering. From the top two panels of Fig. 6, one observes that the number density of electrons in the quantum well gradually rises as U_b increases. The number density of electrons reaches its maximum when $U_b = 0.12$(V), which corresponds to the peak

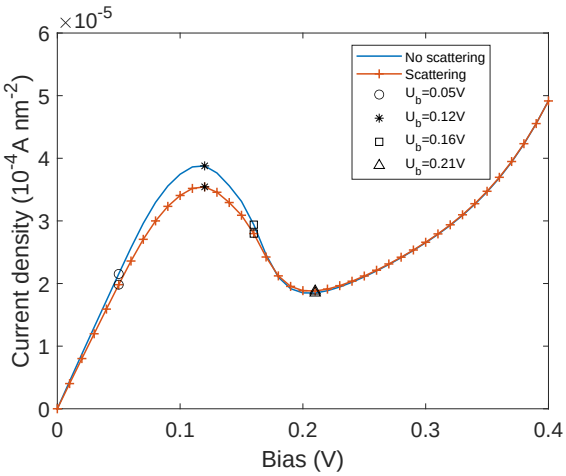

Figure 5: I-V curves for the cases of scattering and no scattering. Four points marked with various symbols pick out current densities at four representative bias values, which are 0.05(V), 0.12(V), 0.16(V) and 0.21(V).

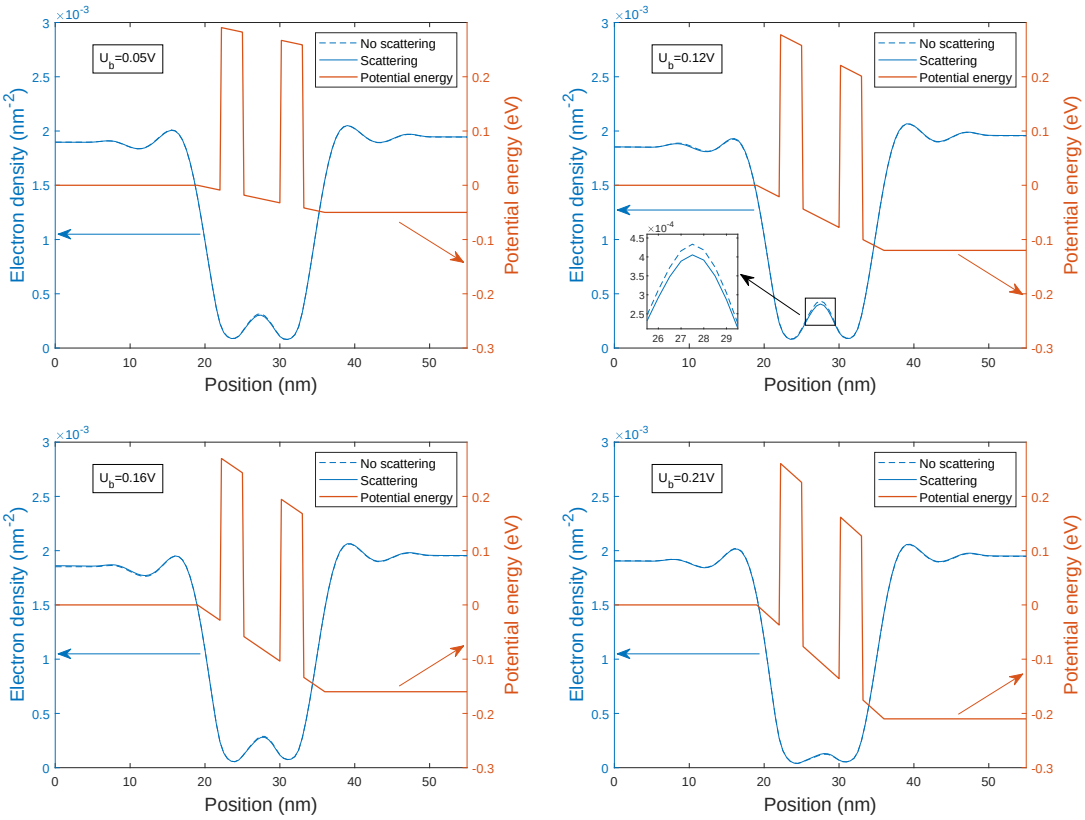

Figure 6: The electron densities corresponding to four representative bias values, i.e., 0.05(V), 0.12(V), 0.16(V) and 0.21(V).

value of current density. However, when U_b further increases, the number density in the well decreases instead, which can be seen from the bottom two panels of Fig. 6. When U_b increases to 0.21(V), the current density reaches its minimum and the corresponding number density of electrons in the well approaches zero. Whether scattering is included or not, the above changes of the electron density can be observed, which demonstrates the resonant tunneling effect. Meanwhile, the electron density in the quantum well decreases in the presence of scattering, which corresponds to the reduction of the current density caused by scattering as shown in Fig. 5. For a more detailed observation, we provide an enlarged view of the electron density in the well for $U_b = 0.12$(V) in Fig. 6, where this phenomenon is more evident.

4.3. Influence of the scattering mechanism on the RTD

To deeply explore the effects of scattering depicted in Figs. 5 and 6, we simulate the stationary Wigner function. By applying equations of motion to the SWE, the SWE can be rewritten as

$$\dot{x}\frac{\partial f(x,k)}{\partial x} + \dot{k}\frac{\partial f(x,k)}{\partial k} = 0,$$

where $\dot{x} = k\hbar/m^*$ and

$$\dot{k} = \frac{\theta[f](x,k) - S[f](x,k)}{\partial f(x,k)/\partial k}.$$

$\partial_t f$ vanishes in the reformulated SWE since we do not distinguish between the solution of the SWE and the steady-state solution of the transient Wigner equation. Therefore, analogous to the Liouville's theorem in classical mechanics, the Wigner distribution function in the phase-space remains constant along the statistics of trajectories of electrons [12, 13]. In Figs. 7 and 8, we show contour lines of the Wigner function corresponding to the solution of the SWE, which can be regarded as long-time statistics of trajectories of electrons described by the transient Wigner equation, according to the discussion made before.

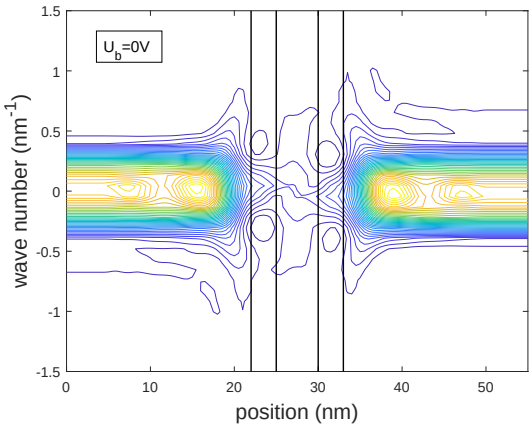

Figure 7: Contour lines of the steady-state distribution function $f(x,k)$ when $U_b = 0$(V).

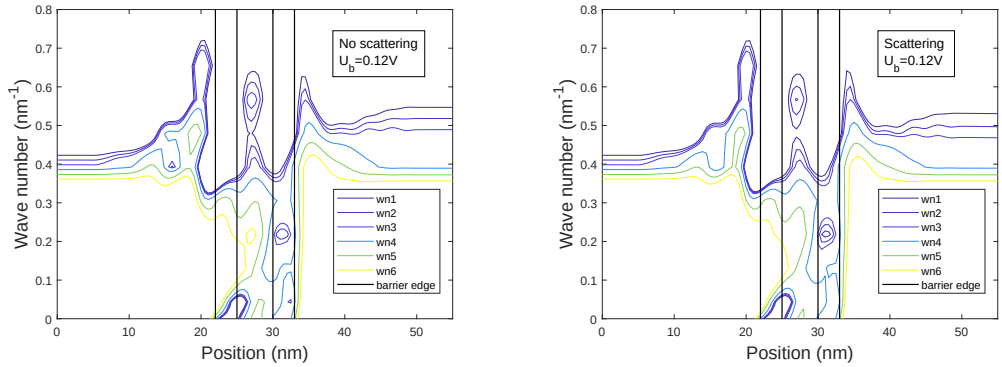

Figure 8: Six specific contour lines of the steady-state solution when $U_b = 0.12$(V). The number following the 'wn' is a trajectory label.

Fig. 7 presents the steady-state solution $f(x, k)$ when $U_b = 0$(V). Four vertical solid black lines mark the edges of the double potential barriers, consistent with the RTD described in Fig. 2. The magnitudes of the wave numbers of phase-space trajectories, which can cross the potential barriers and the quantum well, increase both before reaching the first barrier and upon entering the quantum well. As displayed in Fig. 7, there are closed loops in the barriers and the doping regions, where some trajectories are trapped. Specifically, closed loops in the barriers indicate that the wave number k of the corresponding trajectories suddenly changes from positive to negative or from negative to positive. The positivity or negativity of k represents the direction of the trajectories. Meanwhile, some phase-space trajectories with low wave numbers that are unable to cross the device are reflected back.

To clearly explore the reasons for changes in the current density and the number density caused by scattering, we observe the steady-state solution, specifically when $U_b = 0.12$(V). As displayed in Fig. 8, trajectories with six incident wave numbers are focused on, and only the half-plane with $k > 0$ is shown. The blue line marked with 'wn4' crosses the whole region of the device continuously without scattering, which suggests that the corresponding phase-space trajectories reach the other boundary. Whereas, the blue line is broken with scattering, and the trajectories do not cross the second barrier. This comparison implies two points in the presence of scattering: (1) trajectories that can cross the device decrease, thus, the current density decreases, which is consistent with the observation seen in Fig. 5; (2) the incident wave number k required for crossing the device increases with scattering, and the probability that trajectories which have crossed the first barrier can also cross the second barrier increases. Consequently, the number density of electrons in the quantum well decreases, which is observed in Fig. 6.

5. Conclusion

The USOR-like iterative method is proposed for the SWE in this paper. The proposed method, which still keeps the explicit computational cost, uses as many updated val-

ues of the Wigner function as possible when calculating the pseudo-differential term, and the advection term is considered implicitly. It is numerically validated that the USOR-like iterative method significantly improves the convergence range and the computational efficiency. We study an RTD with double barriers by the USOR-like iterative method. The typical phenomena of the RTD, including the NDR, the resonant tunneling effect and the effects of scattering, are simulated successfully.

Acknowledgments

This research was supported in part by the NSFC (Grant Nos. 12171035, 12131001, 12271035, 12471378), by the Beijing Municipal Natural Science Foundation (Grant No. 1232018), and by the Natural Science Foundation of Guangdong Province of China (Grant No. 2024A1515010356).

References

[1] A. ARNOLD, H. LANGE, AND P. F. ZWEIFEL, *A discrete-velocity, stationary Wigner equation*, J. Math. Phys. 41 (2000), 7167–7180.
[2] L. BARLETTI AND P. F. ZWEIFEL, *Parity-decomposition method for the stationary Wigner equation with inflow boundary conditions*, J. Comput. Theor. Transp. 30 (2001), 507–520.
[3] B. A. BIEGEL AND J. D. PLUMMER, *Comparison of self-consistency iteration options for the Wigner function method of quantum device simulation*, Phys. Rev. B 54 (1996), 8070–8082.
[4] Z. CAI, Y. FAN, R. LI, T. LU, AND Y. WANG, *Quantum hydrodynamic model by moment closure of Wigner equation*, J. Math. Phys. 53 (2012), 103503.
[5] L. L. CHANG, L. ESAKI, AND R. TSU, *Resonant tunneling in semiconductor double barriers*, Appl. Phys. Lett. 24 (1974), 593–595.
[6] X. CHEN, *On convergence of SOR methods for nonsmooth equations*, Numer. Linear Algebra Appl. 9 (2001), 81–92.
[7] A. DORDA AND F. SCHÜRRER, *A WENO-solver combined with adaptive momentum discretization for the Wigner transport equation and its application to resonant tunneling diodes*, J. Comput. Phys. 284 (2015), 95–116.
[8] W. R. FRENSLEY, *Wigner-function model of a resonant-tunneling semiconductor device*, Phys. Rev. B 36 (1987), 1570–1580.
[9] W. R. FRENSLEY, *Boundary conditions for open quantum systems driven far from equilibrium*, Rev. Mod. Phys. 62 (1990), 745–791.
[10] H. K. GUMMEL, *A self-consistent iterative scheme for one-dimensional steady state transistor calculations*, IEEE Trans. Electron Dev. 11 (1964), 455–465.
[11] M. HILLERY, R. F. O'CONNELL, M. O. SCULLY, AND E. P. WIGNER, *Distribution functions in physics: Fundamentals*, Phys. Rep. 106 (1984), 121–167.
[12] K. L. JENSEN AND F. A. BUOT, *Numerical calculation of particle trajectories and tunneling times for resonant tunneling barrier structures*, Appl. Phys. Lett. 55 (1989), 669–671.
[13] K. L. JENSEN AND F. A. BUOT, *The methodology of simulating particle trajectories through tunneling structures using a Wigner distribution approach*, IEEE T. Electron Dev. 38 (1991), 2337–2347.

[14] H. JIANG, W. CAI, AND R. TSU, *Accuracy of the Frensley inflow boundary condition for Wigner equations in simulating resonant tunneling diodes*, J. Comput. Phys. 230 (2011), 2031–2044.
[15] H. JIANG, T. LU, AND W. ZHANG, *A hybrid sinc-Galerkin/finite-difference method for the time-dependent Wigner equation*, J. Comput. Appl. Math. 409 (2022), 114152.
[16] A. JÜNGEL, *Transport Equations for Semiconductors*, in: Lecture Notes in Physics, Springer, 2009.
[17] N. C. KLUKSDAHL, A. M. KRIMAN, D. K. FERRY, AND C. RINGHOFER, *Self-consistent study of the resonant-tunneling diode*, Phys. Rev. B 39 (1989), 7720–7735.
[18] H. KOSINA, M. NEDJALKOV, AND S. SELBERHERR, *Solution of the space-dependent Wigner equation using a particle model*, Monte Carlo Methods Appl. 10 (2004), 359–368.
[19] R. LI, T. LU, AND Z. SUN, *Parity-decomposition and moment analysis for stationary Wigner equation with inflow boundary conditions*, Front. Math. China 12 (2017), 907–919.
[20] R. LI, T. LU, Y. WANG, AND W. YAO, *Numerical validation for high order hyperbolic moment system of Wigner equation*, Commun. Comput. Phys. 15 (2014), 569–595.
[21] T. LU AND Z. SUN, *Singularity-free numerical scheme for the stationary Wigner equation*, J. Comput. Math. 37 (2019), 170–183.
[22] D. QUERLIOZ, P. DOLLFUS, V.-N. DO, A. BOURNEL, AND V. L. NGUYEN, *An improved Wigner Monte-Carlo technique for the self-consistent simulation of RTDs*, J. Comput. Electron. 5 (2006), 443–446.
[23] M. A. REED, J. W. LEE, AND H. TSAI, *Resonant tunneling through a double GaAs/AlAs superlattice barrier, single quantum well heterostructure*, Appl. Phys. Lett. 49 (1986), 158–160.
[24] C. RINGHOFER, *A spectral method for the numerical simulation of quantum tunneling phenomena*, SIAM J. Numer. Anal. 27 (1990), 32–50.
[25] S. SHAO, T. LU, AND W. CAI, *Adaptive conservative cell average spectral element methods for transient Wigner equation in quantum transport*, Commun. Comput. Phys. 9 (2011), 711–739.
[26] Z. SUN, W. YAO, AND T. LU, *Optimization modeling and simulating of the stationary Wigner inflow boundary value problem*, J. Sci. Comput. 85 (2020), 21.
[27] V. SVERDLOV, A. GEHRING, H. KOSINA, AND S. SELBERHERR, *Quantum transport in ultra-scaled double-gate MOSFETs: A Wigner function-based Monte Carlo approach*, Solid State Electron. 49 (2005), 1510–1515.
[28] L. WANG, Q. LIU, AND X. ZHOU, *Convergence of the modified SOR-Newton method for non-smooth equations*, Int. J. Comput. Math. 90 (2013), 1535–1545.
[29] E. P. WIGNER, *On the quantum correction for thermodynamic equilibrium*, Phys. Rev. 40 (1932), 749–759.
[30] M. U. ZAPATA, F. J. HERNANDEZ-LOPEZ, AND R. I. BALAM, *A parallel unstructured multi-color SOR solver for 3D Navier-Stokes equations on graphics processing units*, Comput. Fluids 260 (2023), 105909.
[31] H. ZHAN, Z. CAI, AND G. HU, *The Wigner function of ground state and one-dimensional numerics*, J. Comput. Phys. 449 (2022), 110780.